Assembly of Three-Dimensional Hetero-Epitaxial ZnO/ZnS Core/Shell Nanorod and Single Crystalline Hollow ZnS Nanotube Arrays

Xing Huang,[†,‡,§] Meng Wang,[†,§] Marc-Georg Willinger,[‡] Lidong Shao,[‡] Dang Sheng Su,[‡,∥] and Xiang-Min Meng*[,†]

[†]Key Laboratory of Photochemical Conversion and Optoelectronic Materials, Technical Institute of Physics and Chemistry, Chinese Academy of Sciences, 29 Zhongguancun East Road, 100190 Beijing, People's Republic of China, [‡]Department of Inorganic Chemistry, Fritz Haber Institute of the Max Planck Society, Faradayweg 4–6, 14195 Berlin, Germany, [∥]Shenyang National Laboratory for Materials Science, Institute of Metal Research, Chinese Academy of Science, 72 Wenhua Road, 110016 Shenyang, People's Republic of China, and [§]Graduate School of Chinese Academy of Sciences, 19A Yuquan Road, 100049 Beijing, People's Republic of China

ABSTRACT Hetero-epitaxial growth along three-dimensional (3D) interfaces from materials with an intrinsic large lattice mismatch is a key challenge today. In this work we report, for the first time, the controlled synthesis of vertically aligned ZnO/ZnS core/shell nanorod arrays composed of single crystalline wurtzite (WZ) ZnS conformally grown on ZnO rods along 3D interfaces through a simple two-step thermal evaporation method. Structural characterization reveals a "$(01\bar{1}0)_{ZnO}//(01\bar{1}0)_{ZnS}$ and $[0001]_{ZnO}//[0001]_{ZnS}$" epitaxial relationship between the ZnO core and the ZnS shell. It is exciting that arrays of single crystalline hollow ZnS nanotubes are also innovatively obtained by simply etching away the inner ZnO cores. On the basis of systematic structural analysis, a rational growth mechanism for the formation of hetero-epitaxial core/shell nanorods is proposed. Optical properties are also investigated *via* cathodoluminescence and photoluminescence measurements. Remarkably, the synthesized ZnO/ZnS core/shell heterostructures exhibit a greatly reduced ultraviolet emission and dramatically enhanced green emission compared to the pure ZnO nanorods. The present single-crystalline heterostructure and hollow nanotube arrays are envisaged to be highly promising for applications in novel nanoscale optoelectronic devices, such as UV-A photodetectors, lasers, solar cells, and nanogenerators.

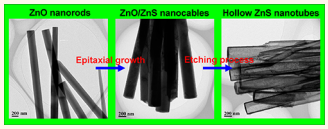

KEYWORDS: heterostructures · single crystalline · ZnS/ZnS core/shell · hetero-epitaxial · ZnS nanotubes · wurtzite structure

Component-modulated semiconductor heterostructures, such as superlattices,[1,2] core/shell,[3] and biaxial nanostructures,[4,5] with integrated multifunctionality of disparate components, are increasingly important in the assembly of nanoscale photonic and electronic devices.[1−7] Extensive investigations on the preparation of heterostructures have been carried out for dimension-specific applications by controlling shapes, structures, and components.[1−9] ZnO and ZnS, as important II−VI semiconductors with wide band-gaps of 3.37 and 3.67 eV, have been intensively studied in a wide range of UV sensors, lasers, field emitters, nanogenerators, solar cells, photocatalysis, and so on, owing to their excellent optoelectronic properties.[10−17] Recently, ZnO/ZnS heterostructures have attracted theoretical and experimental interest for showing superior optoelectronic properties to their individual materials due to their type-II band alignments.[7,18−26] However, existing investigations on ZnO/ZnS heterostructures are mainly related to polycrystalline ZnS nanoparticles covered on ZnO or crystallographic inconsistency in terms of orientation between ZnO and ZnS crystals.[4,5,27−37] Systematically controlled assembly of single crystalline ZnO/ZnS heterostructures with epitaxial orientation relationship has so far not been achieved. Especially for three-dimensional (3D) hetero-epitaxial growth, their intrinsic large lattice mismatch along the interfaces and high sensitivity to synthetic conditions are major challenges yet to be overcome.[4,5]

Here, we report for the first time epitaxial growth of ZnS single crystalline shells onto vertically aligned ZnO nanorod arrays to form arrays of ZnO/ZnS core/shell nanocables *via* a simple two-step thermal evaporation method. Excitingly, single crystalline WZ structured ZnS nanotube arrays are also innovatively synthesized by selectively etching away the inner ZnO cores. Aligned semiconductor nanostructure arrays were chosen because of their ideal geometric shape with respect to applications in photonic and electronic devices, which are characterized by a well-ordered orientation, as well as high aspect and surface-to-volume ratios.[17,20,38,39]

* Address correspondence to mengxiangmin@mail.ipc.ac.cn.

Received for review June 4, 2012 and accepted August 3, 2012.

Published online August 03, 2012
10.1021/nn3024514

The morphologies, compositions, and crystal structures of the hetero-epitaxial core/shell ZnO/ZnS nanorods and the ZnS nanotubes are systematically studied. A growth mechanism is proposed based on the structural characterization and analysis. Optical properties are also investigated and discussed in detail. Using the hetero-epitaxial growth of the ZnS shell on the ZnO core as an example, we demonstrate the possibility of a rational and simple way for establishing 3D hetero-epitaxial nanostructures from materials with an intrinsic large lattice mismatch.

RESULTS AND DISCUSSION

Strategies for the synthesis of the arrays of hetero-epitaxial ZnO/ZnS core/shell nanorods and single crystalline hollow ZnS nanotubes are illustrated in Scheme S1. First, arrays of ZnO nanorods were synthesized on a piece of Si wafer by thermal vaporization of Zn powder in the presence of air in a high-temperature furnace. Scanning electron microscopy (SEM) analysis shows that the synthesized ZnO nanorod has a hexagonal cross section (Supporting Information, Figure S1). X-ray diffraction (XRD) and transmission electron microscopy (TEM) (Figures S1 and S2) reveal that these ZnO nanorods are well-crystallized in the WZ structure with a preferential growth direction of [0001]. Next, ZnS shells were deposited onto the ZnO nanorods by thermal evaporation with a ZnS powder source. Detailed synthetic procedures can be found in the Experimental Section.

The morphology and composition of the product synthesized in the second deposition process were characterized using SEM with energy-dispersive X-ray spectroscopy (EDX). Figure 1a–d, shows low- and high-magnification SEM images of the nano-arrays. It can be clearly seen that the nanorods grew vertically aligned on the Si substrate and had a high density. The individual nanorods possess a perfect hexagonal crystal shape with typical diameters ranging from 250 to 350 nm. The morphology is quite similar to that of the ZnO nanorod prepared in the first step (Figure S1) except for a noticeable increase in diameter. EDX analysis (Figure 1e) of the sample shows that an S peak can be clearly observed in addition to the Zn and O peaks. To further confirm formation of ZnS, an XRD spectrum of the sample was taken, as shown in Figure 1f. Compared with the XRD data recorded from ZnO nanorods (Figure S1), a new peak at around 28.5° is detected, which corresponds to (0002) planes of WZ structured ZnS (JPCDS, 36–1450). These preliminary results demonstrate that the nanorod is composed of ZnO and ZnS.

To further analyze the composition of the product, EDX analysis in a scanning TEM (STEM) was carried out. Figure 2a shows a typical plan-view TEM image of a bundle of the nanorods. Their diameters are significantly larger in comparison to those of the ZnO nanorods (Figure S2), which is consistent with the SEM observations. The dark/bright contrast of the nanocable and its

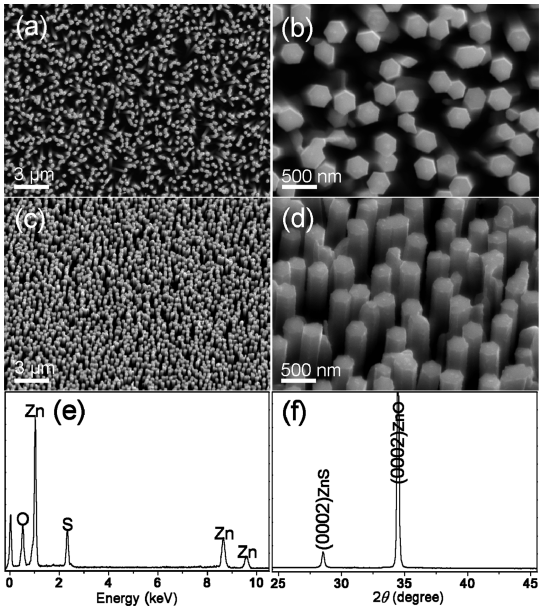

Figure 1. Low- and high-magnification (a, b) top-view and (c, d) tilt-view SEM images of the ZnO/ZnS core/shell nanorod arrays; (e, f) EDX and XRD data collected from the core/shell nanorod arrays.

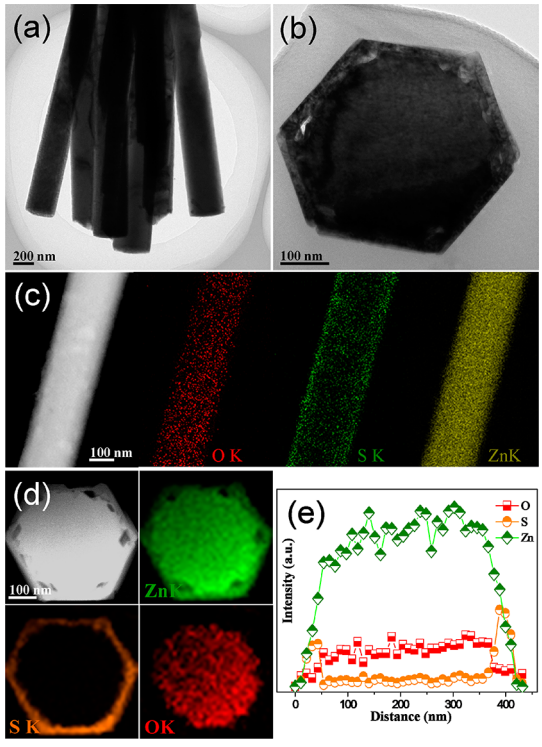

Figure 2. (a) Plan-view and (b) cross-section-view TEM images of the ZnO/ZnS core/shell nanorod; (c) STEM image and EDX elemental mapping from a plan view of core/shell nanorod; (d) HAADF-STEM image and corresponding EDX elemental mapping; (e) EDX line scan data form the core/shell nanorod collected in cross section.

corresponding STEM–EDX elemental mapping shown in Figure 2c reveal that the ZnO nanorod is fully covered with a ZnS layer. To analyze the interfacial relationship

between the two materials, the cross section samples were prepared. Figure 2b gives a cross-sectional TEM image of the product. It can be seen that a hexagonal shell with a thickness of 30 nm is uniformly wrapped around the core region. EDX elemental analysis shows that the core contains only Zn and O, while the shell consists of only Zn and S (Supporting Information, Figure S3). This result is confirmed by combined High Angle Annular Dark Field STEM imaging and EDX elemental mapping (Figure 2d) as well as the line profile analysis (Figure 2e) of the cross section. Clearly, the O element signal is confined to the core region, while S is detected in the hexagonal shell region. In the case of Zn, a homogeneous signal was observed throughout the entire cross section.

To investigate the intrinsic crystal structure of the core/shell nanorods, high-resolution TEM (HRTEM) and selected-area electron diffraction (SAED) were performed. Figure 3a shows an HRTEM image of the interface between the inner ZnO core and ZnS shell along the [2−1−10] direction, as evidenced by its SAED pattern (inset of Figure 3a). Due to the thickness, the contrast of the lattice fringes in the core region of the rod is weak. However, the interface between the core and shell, marked with a white dashed line, can be clearly identified. The corresponding SAED pattern shows two aligned sets of diffraction spots, which can be indexed, respectively, to the WZ structured ZnO and ZnS with an epitaxial orientation relationship: $(0002)_{ZnO}//(0002)_{ZnS}$, $[01-10]_{ZnO}//[01-10]_{ZnS}$. This is schematically illustrated with a relaxed atomic model in Figure 3c. As can be seen in the HRTEM image, the lattice mismatch between the core and shell structure leads to numerous stacking faults along the ZnS [0001] direction. This is also evidenced by the streaks along the diffraction spots of the ZnS shell. Nevertheless, despite the stacking faults, the lattice spacing of 0.31 nm in the shell can be distinguished. It corresponds to (0002) planes of WZ structured ZnS, as shown in Figure 3a.

It is known that the lattice parameters for WZ structured ZnO (JPCDS, 36−1451) and ZnS (JPCDS, 36−1450) are a = 0.3249 nm and c = 0.5206 nm, and a = 0.3820 nm and c = 0.6257 nm, respectively. The lattice mismatch between $(0001)_{ZnO}$ and $(0001)_{ZnS}$ is as high as 20.19%. This would lead to tensile and compressive stress in the ZnO core and the ZnS shell, respectively. This mismatch stress field would increase as the shell thickness increases. Because the ZnO nanorods are synthesized before the establishment of the stress field, we do not expect the mismatch stress field would cause significant change in its crystallinity and defect density (Supporting Information, Figure S4). On the other hand, the ZnS shell reaches a certain critical thickness; the built-up stress can cause structural changes for releasing the stress. As a result, a high density of stacking faults is generated during the radial growth of the ZnS shell, thereby gradually releasing the mismatch strain energy.[5,19]

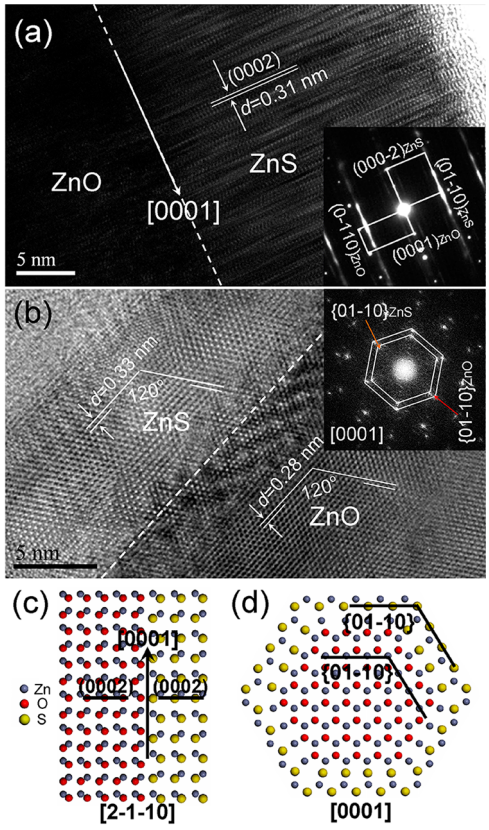

Figure 3. (a) Plan-view HRTEM image, showing the interface of ZnO and ZnS, inset shows the corresponding SAED pattern; (b) Cross-section-view HRTEM image of core/shell nanorod, inset shows the corresponding selected-area Fast Fourier Transform pattern; (c, d) Relaxed atom models illustrated from [2−1−10] (plan-view) and [0001] (cross-section-view) directions, respectively.

Figure 3b presents a cross section HRTEM image of a core/shell nanorod viewed along the [0001] direction. The labeled interplanar distances of 0.28 and 0.33 nm in the core and the shell regions correspond to the lattice fringes of {01−10} planes of WZ structured ZnO and ZnS, respectively. The inset of Figure 3b shows a selected-area Fast Fourier Transform of the HRTEM image. It consists of two well-aligned sets of hexagonal spots, corresponding to the ZnO and the ZnS WZ lattices, respectively. An epitaxial relationship between WZ ZnO and ZnS is identified: $(01-10)_{ZnO}//(01-10)_{ZnS}$ and $[0001]_{ZnO}//[0001]_{ZnS}$, as schematically illustrated in Figure 3d. This result agrees well with the previous analysis in Figure 3a. It is noteworthy that the ZnS shell is single crystalline and preserves the crystal structure characteristic and crystallographic orientation of the initial ZnO core. This is quite different from the previous studies on the ZnO/ZnS heterostructure system,[4,5,27−37] which are either characterized by the polycrystalline nature of ZnS nanoparticles sheathed on the ZnO or inconsistent in crystallographic orientation between ZnO and ZnS crystals.

Based on the above observations and analyses, a combination of three different processes, namely a

hydrogen-assisted thermal evaporation process, a substitution reaction and a homoepitaxial growth process can be used to explain the obtained heterostructures (Figure 4). In the beginning, ZnS powder was evaporated with the assistance of H_2 in the high temperature zone (700 °C) to form Zn and H_2S vapors by a thermal evaporation process[40] (eq 1). The produced vapors were then transferred downstream by the carrier gas and reacted with the previously prepared ZnO nanorods in the low temperature zone (600 °C) to form a thin ZnS layer on the surface of ZnO nanorods (eq 2) by a substitution reaction, that is, O^{2-} was exchanged for S^{2-} on the surface of ZnO nanorods,[35,36] thus, the newly formed ZnS layer can preserve the WZ structure characteristic and crystallographic orientation of ZnO cores.[41] With prolonged time, the prefabricated ZnS layer would limit the accessibility of oxygen and, hence, disable further proceeding of the substitution reaction. Instead, the newly formed layer would serve as substrate for the homo-epitaxial growth of ZnS *via* the vapor−solid mechanism[40,42] (eq 3). As a result, single-crystalline WZ structured ZnS nanostructures would be epitaxially grown on the ZnO nanorods to form arrays of ZnO/ZnS core/shell nanorods.

$$ZnS(s, g) + H_2(g) \xrightarrow{700^{\circ}C} Zn(g) + H_2S(g) \quad (1)$$

$$ZnO(s) + H_2S(g) \xrightarrow{600^{\circ}C} ZnS(s) + H_2O(g) \quad (2)$$

$$Zn(g) + H_2S(g) \xrightarrow{600^{\circ}C} ZnS(s) + H_2(g) \quad (3)$$

To evaluate optoelectronic properties of the products, cathodoluminescence (CL) was investigated at room temperature (RT; Figure 5). Inset of Figure 5 is the UV region of the spectra. For pure ZnO, a relatively sharp UV emission (378 nm), ascribed to excitonic recombinations at the near-band edge (NBE), together with a broad deep-level (DL) emission centered at around 514 nm, which is commonly believed to originate from the radiative recombinations of the holes with electrons belonging to the oxygen vacancies of the surface,[43] were clearly identified. Compared with the bare ZnO nanorods, ZnS-coated core/shell nanorods exhibit a strongly reduced UV emission and a dramatically enhanced DL emission. Obviously, the UV and DL emission peaks are attributed to the emissions of ZnO nanorods within ZnO/ZnS core/shell nanorods. The reduction of UV emission after ZnS coating seems to agree with the charge separation mechanism of type-II band alignment that holes transfer from the core to shell, which would quench the UV emission to a certain extent.[29] However, if this mechanism holds true for the reduction of UV emission in the ZnO/ZnS core/shell nanorods, one would expected a similarly decreased DL emission rather than a strongly enhanced one.[20] Nevertheless, previous studies suggest that the

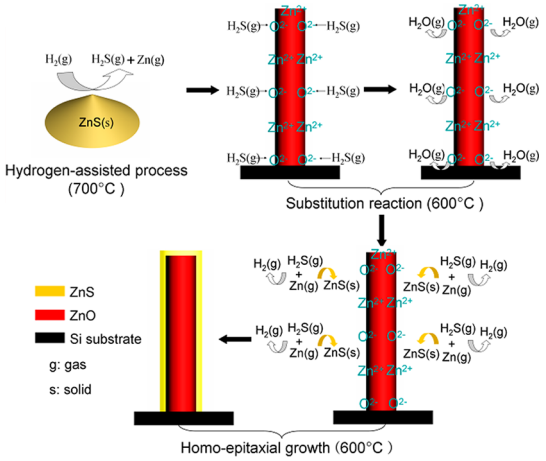

Figure 4. Schematic illustration of the growth mechanism for epitaxial growth of a single crystalline WZ structured ZnS shell on ZnO nanorods.

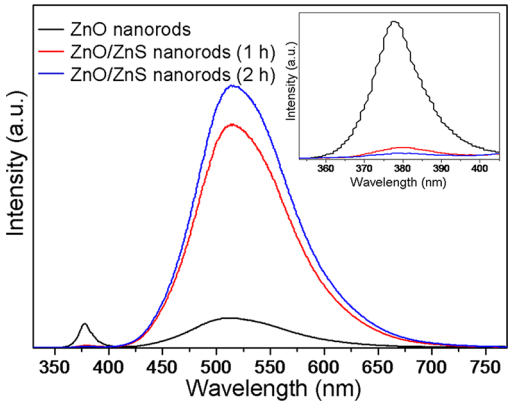

Figure 5. CL spectra obtained at RT from pure ZnO nanorods and ZnO/ZnS core/shell nanorods. The 1 and 2 h stand for the deposition time of ZnS on ZnO nanorods at the temperature of 600 °C.

DL emission is surface-related due to the surface dominance of the defects in the case of nanowires.[43,44] Furthermore, the intensity of DL emission increases at the expense of the NBE emission and is expected to quench NBE emission in the extreme cases.[44,45] Hence, we infer that an increased number of oxygen vacancies at the ZnO surface introduced during the coating process combined with defects resulting from the lattice mismatch along the interface are responsible for the reduction of the UV emission and simultaneous enhancement of the DL emission.[24,46] Same phenomenon was also observed in RT photoluminescence measurements (Figure S5). Although more studies are needed to understand the luminescence mechanisms of such core/shell heterostructures, the present results indeed demonstrate successful tuning of the optical properties.

A simple etching process in an acetic acid solution can be used to dissolve the inner ZnO core and obtain arrays of single crystalline hollow ZnS nanotubes. Low-magnification SEM images (Figure S6) show that ZnS tubes are aligned perpendicularly to the silicon

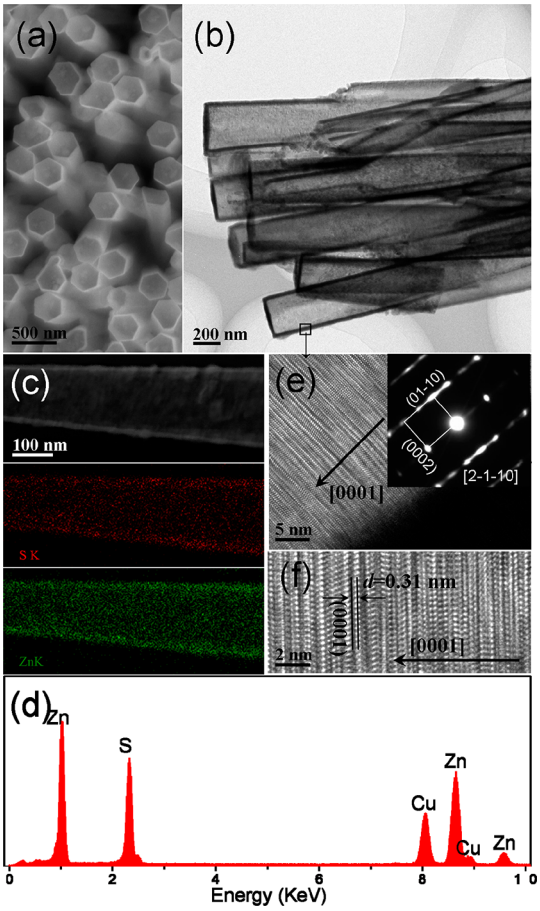

Figure 6. (a) Top-view SEM image, showing a hexagonal shape of cross section of ZnS tubes; (b) Plan-view TEM image of ZnS tubes; (c, d) Elemental mapping and EDX analysis; (e) HRTEM image recorded from the rectangle region in (b); (f) Enlarged HRTEM image of (e).

substrate's surface with a good uniformity. The density of nanotubes is high, and the nanotubes are geometrically well−defined. A top-view SEM image in Figure 6a clearly shows that the synthesized ZnS nanotubes have hexagonal cross sections. The inner diameters of tubes measured from the recorded images are about 200−300 nm, in good accordance with the diameters of the ZnO template. It is interesting to note that these tube ends are closed at the top (Figure 6b), which demonstrates that the ZnO rods were fully coated by ZnS during the epitaxial growth process, that is, not only were the side surfaces covered, but also the tops of the ZnO rods. The inner and outer surfaces of the ZnS nanotube are smooth and the thickness of the wall and the cap is estimated to be in the range of 25 to 35 nm. Elemental composition of the tube was further determined by STEM-EDX (Figure 6c). It was found that the tube contained only Zn and S (Figure 6d), both homogenously distributed throughout the whole region of the tube. Figure 6e shows an HRTEM image and its corresponding SAED pattern (inset of Figure 6e) recorded from the indicated area in Figure 6b. The SAED pattern with an incident electron beam parallel to [2−1−10] reveals a single-crystalline nature of WZ structured ZnS, which grows along the [0001] direction. Although stacking faults are found in the tube, the enlarged image (Figure 6f) exposes the dominant (0002) planes of WZ-structured ZnS with an interplanar distance of 0.31 nm. To the best of our knowledge, it is the first time that uniformly structured hollow ZnS nanotube arrays have been obtained in single crystalline form. The ideal geometric shape, well ordered-orientation and high surface−volume ratio of the obtained hollow ZnS nanotube arrays combined with the single-crystalline nature will benefit its possible applications in various photonic and electronic nanodevices.[17,47]

CONCLUSIONS

Morphology and structure controlled synthesis of vertically aligned and orientation ordered heteroepitaxial ZnO/ZnS core/shell nanorod arrays has been achieved *via* a simple two-step thermal evaporation method. The ZnS shell is single crystalline and preserves the crystal structure and orientation of the ZnO core. The epitaxial relationship between the WZ-structured ZnO core and the ZnS shell is identified to be $(01-10)_{ZnO}//(01-10)_{ZnS}$ and $[0001]_{ZnO}//[0001]_{ZnS}$. A mechanism for the conformal and epitaxial growth of ZnS on the ZnO nanorods has been proposed. The growth involves a hydrogen-assisted thermal evaporation process, a substitution reaction and a homoepitaxial growth process. Single-crystalline hollow ZnS nanotube arrays with WZ structure have also been innovatively obtained by selectively etching away the inner ZnO cores using an acetic acid solution. The CL and PL properties demonstrate successful tuning of the optical properties of ZnO nanostructures by forming ZnO/ZnS heterostructures. The as-synthesized ZnO/ZnS heterostructures and hollow ZnS nanotubes may provide ideal systems for fundamental research and are highly promising building blocks for nanoscale device applications. Due to its simplicity and efficiency, one can expect that this approach could be similarly used to fabricate varieties of heterostructures made of materials with an intrinsic large lattice mismatch and single-crystalline hollow nanostructures.

EXPERIMENTAL SECTION

Synthesis of arrays of ZnO and ZnO/ZnS core/shell nanorods was performed in a vacuum tube mounted inside a two-zone, high-temperature furnace.

Synthesis of ZnO Nanorod Arrays. First, Zn powder (analytical grade) was placed in a ceramic boat covered with a piece of silicon wafer. The boat was then put at the high-temperature zone of a quartz tube. After pumping down the pressure in the

tube to 0.1 Pa, air with a constant rate of 30 sccm (standard cubic centimeters per minute) was flowing into the tube. The pressure of the tube was maintained at 100 Pa, and the boat was heated to 600 °C and maintained for 90 min. After that, the furnace was naturally cooled down to room temperature and ZnO nanorod arrays were synthesized on the silicon wafer.

Synthesis of Hetero-Epitaxial ZnO/ZnS Core/Shell Nanorod Arrays. Second, we put ZnS powder (analytical grade) at the high-temperature zone of the quartz tube and the silicon wafer with ZnO nanorods at a lower temperature zone of the quartz tube. High-purity argon mixed with 5% hydrogen with a constant rate of 45 sccm was flowing into the tube. Deposition was carried out by heating the ZnS to about 700 °C and keeping the silicon wafer with ZnO nanorods at 600 °C. Pressure in the tube was maintained at 480 Pa during the whole experiment. After the deposition process, the furnace was then naturally cooled down to room temperature and ZnO/ZnS core/shell nanorod arrays were then obtained on the silicon wafer.

Preparation of Hollow ZnS Nanotube Arrays. Finally, hollow ZnS nanotube arrays were obtained by immersing ZnO/ZnS core/shell nanorod arrays in an acetic acid solution (20 wt %) for 6 h at room temperature to completely remove the inner ZnO cores, and then they were dried in air.

Preparation of Cross Section of ZnO/ZnS Core/Shell Nanorods. The core/shell nanorods were embedded in epoxy and glued between two silicon dummies. This sandwich was thinned from both sides with SiC grinding paper and diamond lapping film up to 10 μm thickness. After gluing on an aperture hole, the TEM cross section sample was prepared by ion beam etching in a PIPS 619 system (Precision Ion Polishing System, Gatan) with 4 kV and Ar from both sides up to the electron transparency.

Characterization and Measurements. SEM images of the samples were taken on a Hitachi S−4300 scanning electron microscope operated at 10 kV. X-ray diffraction patterns of the samples were recorded on a Bruker D8 Focus powder X-ray diffractometer using Cu Kα radiation (λ = 1.5418 Å). TEM and HRTEM images were recorded on a JEM-2100F operated at 200 kV and a FEI Cs-corrected Titan 80−300 microscope operated at 300 kV with a Gatan energy filter. Cathodoluminescence and photoluminescence spectra were collected on Quanta 200F SEM operated at 15 kV and pulsed Nd:YAG laser (Quanta−Ray INDI Series) with an excitation wavelength of 266 nm, respectively.

Conflict of Interest: The authors declare no competing financial interest.

Acknowledgment. This work received financial support from the National Natural Science Foundation of China (21073212) and 973 Project (2009CB623003). We thank A. K. Hoffmann for the preparation of cross section of core/shell nanorods and S. Chen for the photoluminescence test.

Supporting Information Available: Schematic illustration of the fabrication process; EDX and XRD spectra, SEM, TEM, and HRTEM images of ZnO nanorods; EDX data collected from the core and shell regions of cross section sample; SAED patterns and PL spectra recorded from ZnO and ZnO/ZnS core/shell nanorods; EDX, XRD, and SEM data of hollow ZnS nanotubes. This material is available free of charge *via* the Internet at http://pubs.acs.org.

REFERENCES AND NOTES

1. Robinson, R. D.; Sadtler, B.; Demchenko, D. O.; Erdonmez, C. K.; Wang, L. W.; Alivisatos, A. P. Spontaneous Superlattice Formation in Nanorods through Partial Cation Exchange. *Science* **2007**, *317*, 355–358.
2. Fang, X. S.; Bando, Y.; Gautam, U. K.; Zhai, T. Y.; Gradecak, S.; Golberg, D. Heterostructures and Superlattices in One-Dimensional Nanoscale Semiconductors. *J. Mater. Chem.* **2009**, *19*, 5683–5689.
3. Lauhon, L. J.; Gudiksen, M. S.; Wang, D. L.; Lieber, C. M. Epitaxial Core-Shell and Core-Multishell Nanowire Heterostructures. *Nature* **2002**, *420*, 57–61.
4. Fan, X.; Zhang, M. L.; Shafiq, I.; Zhang, W. J.; Lee, C. S.; Lee, S. T. ZnS/ZnO Heterojunction Nanoribbons. *Adv. Mater.* **2009**, *21*, 2393–2396.
5. Yan, J.; Fang, X. S.; Zhang, L. D.; Bando, Y.; Gautam, U. K.; Dierre, B.; Sekiguchi, T.; Golberg, D. Structure and Cathodoluminescence of Individual ZnS/ZnO Biaxial Nanobelt Heterostructures. *Nano Lett.* **2008**, *8*, 2794–2799.
6. Zhou, J.; Liu, J.; Wang, X. D.; Song, J. H.; Tummala, R.; Xu, N. S.; Wang, Z. L. Vertically Aligned Zn_2SiO_4 Nanotube/ZnO Nanowire Heterojunction Arrays. *Small* **2007**, *3*, 622–626.
7. Hu, L. F.; Yan, J.; Liao, M. Y.; Xiang, H.; Gong, J.; X.; Zhang, L. D.; Fang, X. S. An Optimized Ultraviolet-A Light Photodetector with Wide-Range Photoresponse Based on ZnS/ZnO Biaxial Nanobelt. *Adv. Mater.* **2012**, *24*, 2305–2309.
8. Mokari, T.; Rothenberg, E.; Popov, I.; Costi, R.; Banin, U. Selective Growth of Metal Tips onto Semiconductor Quantum Rods and Tetrapods. *Science* **2004**, *304*, 1787–1790.
9. Shen, S. L.; Zhang, Y. J.; Peng, L.; Du, Y. P.; Wang, Q. B. Matchstick-Shaped Ag_2S−ZnS Heteronanostructures Preserving both UV/Blue and Near-Infrared Photoluminescence. *Angew. Chem., Int. Ed.* **2011**, *50*, 7115–7118.
10. Fang, X. S.; Bando, Y.; Shen, G. Z.; Ye, C. H.; Gautam, U. K.; Costa, P. M. F. J.; Zhi, C. Y.; Tang, C. C.; Golberg, D. Ultrafine ZnS Nanobelts as Field Emitters. *Adv. Mater.* **2007**, *19*, 2593–2596.
11. Utama, M. I. B.; Zhang, Q.; Jia, S. F.; Li, D. H.; Wang, J. B.; Xiong, Q. H. Epitaxial II−VI Tripod Nanocrystals: A Generalization of van der Waals Epitaxy for Nonplanar Polytypic Nanoarchitectures. *ACS Nano* **2012**, *6*, 2281–2288.
12. Fang, X. S.; Zhai, T. Y.; Gautam, U. K.; Li, L.; Wu, L. M.; Bando, Y.; Golberg, D. ZnS Nanostructures: From Synthesis to Applications. *Prog. Mater. Sci.* **2011**, *56*, 175–287.
13. Liu, W.; Wang, N.; Wang, R. M.; Kumar, S.; Duesberg, G. S.; Zhang, H. Z.; Sun, K. Atom-Resolved Evidence of Anisotropic Growth in ZnS Nanotetrapods. *Nano Lett.* **2011**, *11*, 2983–2988.
14. Wang, Z. L.; Song, J. H. Piezoelectric Nanogenerators Based on Zinc Oxide Nanowire Arrays. *Science* **2006**, *312*, 242–246.
15. Fang, X. S.; Bando, Y.; Liao, M. Y.; Gautam, U. K.; Zhi, C. Y.; Dierre, B.; Liu, B. D.; Zhai, T. Y.; Sekiguchi, T.; Koide, Y.; et al. Single-Crystalline ZnS Nanobelts as Ultraviolet-Light Sensors. *Adv. Mater.* **2009**, *21*, 2034–2039.
16. Fan, X.; Meng, X. M.; Zhang, X. H.; Shi, W. S.; Zhang, W. J.; Zapien, J. A.; Lee, C. S.; Lee, S. T. Dart-Shaped Tricrystal ZnS Nanoribbons. *Angew. Chem., Int. Ed.* **2006**, *45*, 2568–2571.
17. Fang, X. S.; Wu, L. M.; Hu, L. F. ZnS Nanostructure Arrays: A Developing Material Star. *Adv. Mater.* **2011**, *23*, 585–598.
18. Schrier, J.; Demchenko, D. O.; Wang, L. W.; Alivisatos, A. P. Optical Properties of ZnO/ZnS and ZnO/ZnTe Heterostructures for Photovoltaic Applications. *Nano Lett.* **2007**, *7*, 2377–2382.
19. Wu, X.; Jiang, P.; Ding, Y.; Cai, W.; Xie, S. S.; Wang, Z. L. Mismatch Strain Induced Formation of ZnO/ZnS Heterostructured Rings. *Adv. Mater.* **2007**, *19*, 2319–2323.
20. Wang, K.; Chen, J. J.; Zeng, Z. M.; Tarr, J.; Zhou, W. L.; Zhang, Y.; Yan, Y. F.; Jiang, C. S.; Pern, J.; Mascarenhas, A. Synthesis and Photovoltaic Effect of Vertically Aligned ZnO/ZnS Core/Shell Nanowire Arrays. *Appl. Phys. Lett.* **2010**, *96*, 123105.
21. Lu, M. Y.; Song, J. H.; Lu, M. P.; Lee, C. Y.; Chen, L. J.; Wang, Z. L. ZnO−ZnS Heterojunction and ZnS Nanowire Arrays for Electricity Generation. *ACS Nano* **2009**, *3*, 357–362.
22. Yang, H. Y.; Yu, S. F.; Yan, J.; Zhang, L. D. Wide Bandwidth Lasing Randomly Assembled ZnS/ZnO Biaxial Nanobelt Heterostructures. *Appl. Phys. Lett.* **2010**, *96*, 141115.
23. Liu, W.; Wang, R. M.; Wang, N. From ZnS Nanobelts to ZnO/ZnS Heterostructures: Microscopy Analysis and Their Tunable Optical Property. *Appl. Phys. Lett.* **2010**, *97*, 041916.
24. Gao, P.; Wang, L. Q.; Wang, Y.; Chen, Y. J.; Wang, X. N.; Zhang, G. L. One-Pot Hydrothermal Synthesis of Heterostructured ZnO/ZnS Nanorod Arrays with High Ethanol-Sensing Properties. *Chem.—Eur. J.* **2012**, *18*, 4681–4686.
25. Wang, Z. Q.; Wang, J.; Sham, T. K.; Yang, S. G. Tracking the Interface of an Individual ZnS/ZnO Nano−Heterostructure. *J. Phys. Chem. C* **2012**, *116*, 10375–10381.
26. Wang, F. J.; Liu, J.; Wang, Z. J.; Lin, A. J.; Luo, H.; Yu, X. B. Interfacial Heterostructure Phenomena of Highly Luminescent ZnS/ZnO Quantum Dots. *J. Electrochem. Soc.* **2011**, *158*, H30–H34.

27. Yan, C. L.; Xue, D. F. Conversion of ZnO Nanorod Arrays into ZnO/ZnS Nanocable and ZnS Nanotube Arrays *via* an *In Situ* Chemistry Strategy. *J. Phys. Chem. B* **2006**, *110*, 25850–25855.
28. Shuai, X. M.; Shen, W. Z. A Facile Chemical Conversion Synthesis of ZnO/ZnS Core/Shell Nanorods and Diverse Metal Sulfide Nanotubes. *J. Phys. Chem. C* **2011**, *115*, 6415–6422.
29. Meng, X. Q.; Peng, H. W.; Gai, Y. Q.; Li, J. B. Influence of ZnS and MgO Shell on the Photoluminescence Properties of ZnO Core/Shell Nanowires. *J. Phys. Chem. C* **2010**, *114*, 1467–1471.
30. Hu, Y.; Qian, H. H; Liu, Y.; Du, G. H.; Zhang, F. M.; Wang, L. B.; Hu, X. A Microwave-Assisted Rapid Route to Synthesize ZnO/ZnS Core−Shell Nanostructures *via* Controllable Surface Sulfidation of ZnO Nanorods. *CrystEngComm* **2011**, *13*, 3438–3443.
31. Yu, X. L.; Song, J. G.; Fu, Y. S.; Xie, Y.; Song, X.; Sun, J.; Du, X. W. ZnS/ZnO Heteronanostructure as Photoanode to Enhance the Conversion Efficiency of Dye-Sensitized Solar Cells. *J. Phys. Chem. C* **2010**, *114*, 2380–2384.
32. Jin, C.; Kim, H.; Baek, K.; Lee, C. Effects of Coating and Thermal Annealing on the Photoluminescence Properties of ZnS/ZnO One-Dimensional Radial Heterostructures. *Mater. Sci. Eng., B* **2010**, *170*, 143–148.
33. Yi, R.; Qiu, G. Z.; Liu, X. H. Rational Synthetic Strategy: From ZnO Nanorods to ZnS Nanotubes. *J. Solid State Chem.* **2009**, *182*, 2791–2795.
34. Ahmad, M.; Yan, X. X.; Zhu, J. Controlled Synthesis, Structural Evolution, and Photoluminescence Properties of Nanoscale One-Dimensional Hierarchical ZnO/ZnS Heterostructures. *J. Phys. Chem. C* **2011**, *115*, 1831–1837.
35. Panda, S. K.; Dev, A.; Chaudhuri, S. Fabrication and Luminescent Properties of c-Axis Oriented ZnO−ZnS Core-Shell and ZnS Nanorod Arrays by Sulfidation of Aligned ZnO Nanorod Arrays. *J. Phys. Chem. C* **2007**, *111*, 5039–5043.
36. Wang, X. D.; Gao, P. X.; Li, J.; Summers, C. J.; Wang, Z. L. Rectangular Porous ZnO−ZnS Nanocables and ZnS Nanotubes. *Adv. Mater.* **2002**, *14*, 1732–1735.
37. Dawood, F.; Schaak, R. E. ZnO-Templated Synthesis of Wurtzite-Type ZnS and ZnSe Nanoparticles. *J. Am. Chem. Soc.* **2009**, *131*, 424–425.
38. Shi, L.; Pei, C. J.; Xu, Y. M.; Li, Q. Template-Directed Synthesis of Ordered Single-Crystalline Nanowires Arrays of Cu_2ZnSnS_4 and $Cu_2ZnSnSe_4$. *J. Am. Chem. Soc.* **2011**, *133*, 10328–10331.
39. Xu, J.; Yang, X.; Wang, H. K.; Chen, X.; Luan, C. Y.; Xu, Z. X.; Lu, Z. Z.; Roy, V. A. L.; Zhang, W. Z.; Lee, C. S. Arrays of ZnO/$Zn_xCd_{1-x}Se$ Nanocables: Band Gap Engineering and Photovoltaic Applications. *Nano Lett.* **2011**, *11*, 4138–4143.
40. Jiang, Y.; Meng, X. M.; Liu, J.; Xie, Z. Y.; Lee, C. S.; Lee, S. T. Hydrogen-Assisted Thermal Evaporation Synthesis of ZnS Nanoribbons on a Large Scale. *Adv. Mater.* **2003**, *15*, 323–327.
41. Park, J.; Zheng, H. M.; Jun, Y. W.; Alivisatos, A. P. Hetero-Epitaxial Anion Exchange Yields Single-Crystalline Hollow Nanoparticles. *J. Am. Chem. Soc.* **2009**, *131*, 13943–13945.
42. Lee, K. H.; Lee, S. W.; Vanfleet, R. R.; Sigmund, W. Amorphous Silica Nanowires Grown by the Vapor−Solid Mechanism. *Chem. Phys. Lett.* **2003**, *376*, 498–503.
43. Cheng, C.; Lei, M.; Feng, L.; Wong, T. L.; Ho, K. M.; Fung, K. K.; Loy, M. M. T.; Yu, D. P.; Wang, N. High-Quality ZnO Nanowire Arrays Directly Fabricated from Photoresists. *ACS Nano* **2009**, *3*, 53–58.
44. Shalish, I.; Temkin, H.; Narayanamurti, V. Size-Dependent Surface Luminescence in ZnO Nanowires. *Phys. Rev. B* **2004**, *69*, 245401–245404.
45. Shi, L.; Xu, Y. M.; Hark, S. K.; Liu, Y.; Wang, S.; Peng, L. M.; Wong, K. W.; Li, Q. Optical and Electrical Performance of SnO_2 Capped ZnO Nanowire Arrays. *Nano Lett.* **2007**, *7*, 3559–3563.
46. Zhao, J. W.; Qin, L. R.; Zhang, L. D. Fabrication of ZnS/ZnO Hierarchical Nanostructures by Two-Step Vapor Phase Method. *Mater. Res. Bull.* **2009**, *44*, 1003–1008.
47. Liang, H. W.; Liu, S.; Yu, S. H. Controlled Synthesis of One-Dimensional Inorganic Nanostructures Using Pre-Existing One-Dimensional Nanostructures as Templates. *Adv. Mater.* **2010**, *22*, 3925–3937.